Identification of continuous geomagnetic pulsations

Sebastião Wendell Nobre Moura[1], Raphael Di Carlo Silva dos Santos[1], Giorgio Arlan da Silva Picanço[2]
[1] Universidade Federal do Oeste do Pará (UFOPA)
[2] Instituto Nacional de Pesquisas Espaciais (INPE)

Abstract

The geomagnetic field produces aeronomic phenomena according to the Earth's magnetic latitude. In Brazil we find two important phenomena: the South American Magnetic Anomaly (SAMA) and the Equatorial Electrojet (EEJ). In the equatorial region, the energetic particle precipitation intensifies the Ionospheric ionization, producing intense aeronomic effects, such as the Equatorial Ionization Anomaly (EIA) enhancement. In this context, this study aimed to analyze amplitudes of continuous geomagnetic pulsations (Pc3 and Pc4 type) in magnetic stations located between the EEJ and SAMA latitudes, in the Brazilian region. We acquired data from five magnetic stations during quiet and disturbed days of August, 2018 (based on DST index). The geomagnetic pulsations in equatorial region are mainly related to the type of ionospheric conductivity, such as Cowling's conductivity, contributing for the amplification or damping of Pcs wavelength. Finally, we concluded that the Pc3 and Pc4 amplitudes were influenced by the EEJ behavior.

Introduction

The geomagnetic pulsations are generated by magnetohydrodynamic (MHD) waves, which result from a fluid with high electrical conductivity in the presence of a magnetic field. In this way, these pulsations are in the band of ultra-low frequencies (ULF) and their origins derive from several processes and instabilities on the solar plasma (MCPHERRON, 2005). The pulsations are used mainly for studies of the geomagnetic field and they are classified according to the morphology and wave periods, which are: quasi-sine waves, called continuous pulsations (Pc), and oscillations with a more irregular shape, called irregular pulsations (Pi) (JACOBS et al.,1964).

The geomagnetic pulsations are not just a function of time because the intensity of geomagnetic field presents significant variation in relation to a position on the Earth's surface. The minimum value of magnetic field observed in the SAMA region, for example, is related to the weakening of the field lines and may modify the aeronomic phenomena that occurs in the ionosphere , e.g.: ionospheric airglow (TAVARES AND SANTIAGO, 2002; CAMPBELL, 2003). At the magnetic equator, the field intensity is affected by the EEJ. This phenomenon can be described as an electric current that flows in the daytime ionospheric E-region producing the highest values of the geomagnetic field intensity (SILVA, 2017; KELLEY, 2009;SARMA,1995).

The EEJ has a great influence on geomagnetic pulsations during the solar minimum (SILVA, 2017). The amplification of the signal that represents a magnetic pulse occurs only for the interval belonging to pulsations Pc4 and Pc5 (45-600s), and, at the magnetic equator, the damping of the same signal occurs for the intervals belonging to Pc3 (SHINOHARA et al., 1997). The cause for different observed values found at the magnetic equator is not yet a unified response in literature, however there are hypotheses indicating that these effects are associated with the Cowling conductivity (KIKUCHI; ARAKI, 1979a, b; ITONAGA et al., 1998).

For a better understanding of this phenomenon, this study aims to identify Pc3 and Pc4 signals from several magnetic stations placed in a latitude extent ranging from the SAMA to the EEJ region, during August, 2018, based on the DST index. Then we used data from magnetic stations located near the magnetic equator such as Tatuoca (Brazil), Kourou (French Guiana), Araguatins (Brazil) and San Juan (Puerto Rico). For the identification of Pc3 and Pc4 pulsations we used bandpass filters and spectrograms of the values of the horizontal component of the geomagnetic field.

Geomagnetic pulses

Geomagnetic pulsations are micro variations in the geomagnetic field. They are observed on the Earth's surface and they have wavelength associated with those of ULF. The frequency of these pulsations ranges from 1 mHz to greater than 10 Hz and frequently have amplitudes that reach hundreds of nanoteslas (DUNGEY, 1961).

The pulsations are divided into three distinct frequency bands: low (1 mHz to 10 mHz) medium (10 mHz to 0.1 Hz) and high (0.1 Hz to 10 Hz) and in two types of waves, the continuous (Pc) and irregular pulsations (Pi). Irregular pulsations (Pi) are comparatively shorter in duration and are generally composed of few oscillations decaying in time presenting sinusoidal shape or well-defined spectral peak. The continuous pulsations (Pc) cover the interval with periods of 0.2 to 600 seconds. The cyclotronic frequency of the H^+ ion up to 10 Hz in the magnetosphere is the limit for the frequency of these pulsations (SAMSON, 1991; SIBECK, 1994), while the lower limit,

approximately 1 mHz, is characterized by its propagation time through the magnetosphere (KAMIDE; CHIAN, 2007). Pc pulsations of the Pc4 type are low frequency plasma waves with wavelengths comparable to the dimensions of the magnetosphere (SAMSON, op.cit.). Pc4 pulses have two peaks of amplitudes; one near the aurora zone and the other in sub-aurora zones. At medium latitudes, the occurrence is maximum at noon (SAITO, 1969). They are caused predominantly by instabilities such as Kelvin-Helmholtz´s.

The Pc3 pulses are generated by the impact of the solar wind at the magnetopause. Plasma waves generated by these instabilities are propelled downstream through the bow shock and through the magnetopause to the internal magnetosphere. They are frequent on the dawn with average periods varying and maximized at noon (SAMSON, 1991).

DST Index

The Disturbance Storm Time (DST) index is related to the current in the equatorial region that flows to the Van Allen radiation belt, known as ring current (SIMÕES, 2011). The intensities of geomagnetic storms can be classified according to this index (Table 1) (GONZALEZ et al, 1994; MENDES, 1992).

Geomagnetic storms can be divided into three phases according to the behavior of the DST. The initial phase is preceded or not by a sudden start, lasting for some minutes to a few hours and with an increase in the index to a few hundreds of nT. A main phase, characterized by a decrease in the index value, reaching hundreds of negative nT. And the recovery phase, when the index starts to show undisturbed values indicating the end of the storm. The end of the recovery phase is identified when the DST reaches a value equal to 1/10 the minimum value observed during the main phase of the storm (MENDES, op. cit.; GONZALEZ et al., op.cit;).

INTENSITY	AMPLITUDE (nT)
WEAK	50 < DST ≤ -30
MODERATE	-100 < DST ≤ -50
INTENSE	-250 < DST ≤ -100
VERY INTENSE	DST ≤ -250

Table 1 – Intensity of a geomagnetic storm according to DST index. Adapted from Gonzales et al. (1994).

Data Acquisition

We used, in this study, data from stations located at San Juan (SJG, Puerto Rico), Kourou (KOU, French Guiana), Araguatins (ARA, Tocantins, Brazil) and Tatuoca (TTB, Pará, Brazil). Data of San Juan, Kourou and Araguatins stations were acquired from the worldwide magnetometer network, INTERMAGNET, in partnership with the German Geosciences Research Center (GFZ) and the Brazilian magnetometer network, HUG. Tatuoca data was acquired from the Observatório Nacional (ON) team responsible for the operation of the station.

We chose the year 2018 for the analysis of possible geomagnetic storms. The figure 1 shows the values representative of the temporal variance of the Dst index in August, 2018. We chose stations near and far from effects of ionospheric currents in different latitudes because we intended to study if EEJ could affect the data. The SJG, for example, is a station that is distant from the magnetic equator so it tends to present values which are not affected by EEJ. The nearest stations to equator are located in the Amazon territory, so TTB is more subject to the effects of ionospheric current in its amplitudes. Figure 2 shows the locations of the stations. We standardized the time in Universal Time (UT) in all data of this study.

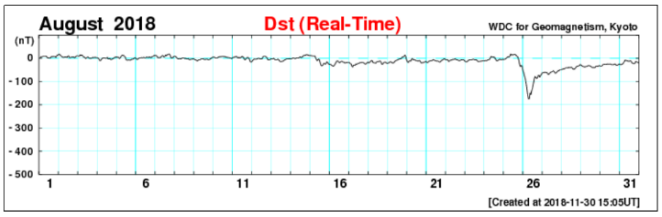

Figure 1 – Time variation in function of DST index for August, 2018. Adapted from Kyoto Observatory of Data Analysis Center for Geomagnetism and Space Magnetism, Kyoto University, Japan.

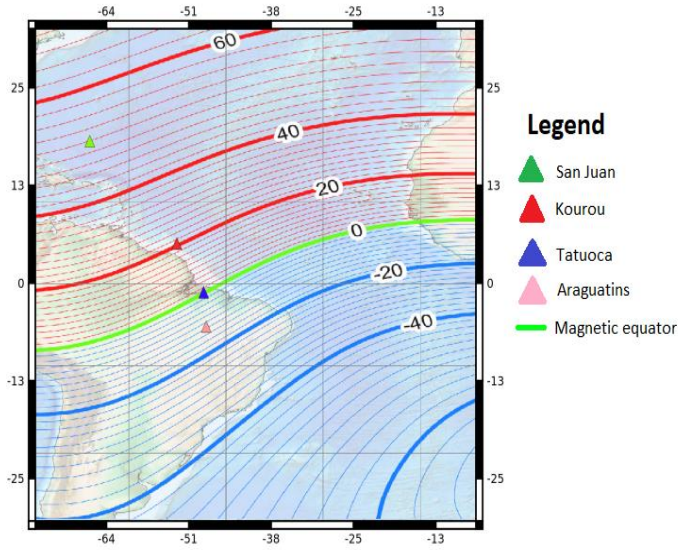

Figure 2 – Location of the geomagnetic stations.

Data filtering

We used several criteria for choosing a period of days to filter and identify the pulsations, which are: data availability, location, sampling rate and the DST index value (PIASSI, 2018). The period that fulfilled all demands was August, 2018. At the end of the month of August we observed a geomagnetic storm that started on the 26th day and lasted until the 31st.

We performed a time series filtering of the horizontal component of the geomagnetic field and, then, we calculated the spectrogram of the values. We used a Butterworth bandpass filter in order to extract the Pc3 and Pc4 pulses frequencies. The table 2 shows the frequencies and periods of each pulse.

PULSE	FREQUENCY INTERVAL (mHz)	PERIOD INTERVAL (s)
Pc3	20-100	40-45
Pc4	6.6 – 22.2	45-150

Table 2 – Frequencies and periods of Pc3 and Pc4 pulses

In order to identify a magnetic pulse, we used the Fourier Transform of a signal, expressed as

$$F(\omega) = \int_0^T f(t)e^{-i\omega t}dt, \qquad (1)$$

where $f(t)$ is the signal in function of time, T is the period of the signal and ω is the angular frequency denoted by $\omega = \frac{2\pi}{T}$. The Fourier Transform (FT) is applied just in stationary signals, however the geomagnetic field values vary in time, so we used the Short-Time Fourier Transform (SFTF) method. It divides a longer time signal into shorter windows of same length and the calculates the Fourier transform on each window separately. First it calculates the FT discretely in a N-elements window $(f_0, \dots, f_{N-1})$, then it moves the window in a fixed time to $(f_1, \dots, f_N)$, and then to the last M values $(f_{N-M}, \dots, f_M)$. It is expressed as

$$F(\tau, \omega) = \int_{-\infty}^{\infty} f(t)w(t-\tau)e^{-i\omega t}dt, \qquad (2)$$

where $w(\tau)$ is the window function and τ is the time index. After the calculation of equation (2) we create the spectrogram.

Results

We analyzed six days of geomagnetic observations divided in two groups: geomagnetically quiet and disturbed days. In order to identify the pulses, we used the criteria of Piassi (2018): A) the pulse must have minimum amplitudes of 0.1 nT and 0.2 nT for Pc3 and Pc4, respectively. B) both amplitudes must present the same waveform in all stations. C) Both pulses must present at least 3 wavecycles.

We searched for pulses in the days 21, 22, 23 (quiet days), 24, 25 and 26 (disturbed days) of August, 2018. We did not find data of the station ARA for the quiet days.

For quiet days we found 8 pulses indicating a Pc3. These pulses were found in the days 21 and 22, the day 23 have not shown any significant pulse that filled the criteria, though. The day 21 shows 6 pulses and day 22 shows 2 pulses (Figure 3 and 4). The figure 5 and 6 show the spectrogram of these days. We realized that at the time 10.2 UT the values indicate the moment the sun emanates charged particles increasing momentarily the intensity of the geomagnetic field. Although they are quiet days, we have found values for dB/Hz ratio of Pc3 pulse near zero. For the day 22 we noticed the pulse at the time 15.6 UT. It can be explained due to a great quantity of coronal mass ejected perpendicularly to the location of the stations. Also, we have observed two anomalous pulses in KOU station due to the intense flow of ionospheric particles in EEJ region.

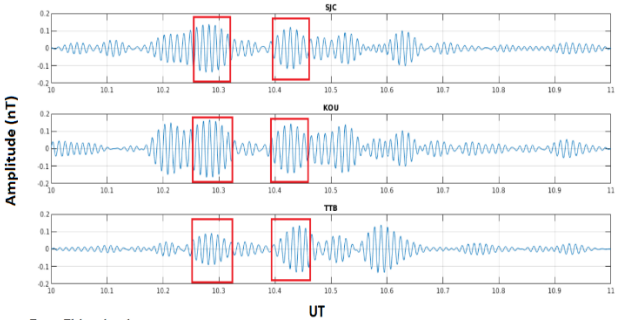

Figure 3 – Identification of Pc3 pulses in the day 21. Red rectangles identify the pulses.

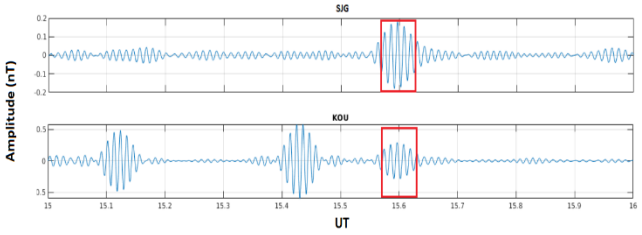

Figure 4 – Identification of Pc3 pulses in the day 22. Red rectangles identify the pulses.

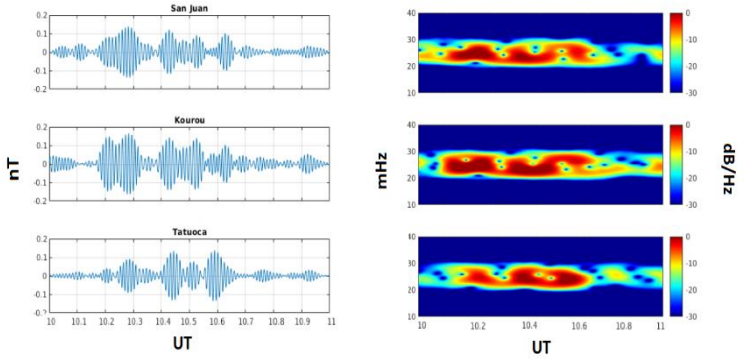

Figure 5 – Pc3 spectrogram of the day 21.

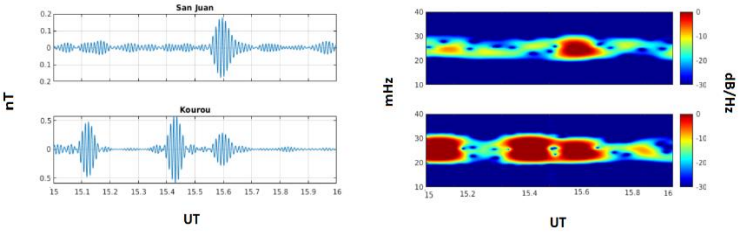

Figure 6 – Pc3 spectrogram of the day 22.

For the disturbed days 26 and 27 we have found 9 Pc3 pulses (Figures 7 and 8, respectively). The day 25 did not show any pulse, we have found noisy values with low amplitudes in all stations, though. The Figure 7 shows two anomalous pulses between 7 UT and 8 UT and they may be related to the geomagnetic storm and the influence of EEJ. Also, we noticed two other Pc3 pulses between 16 UT and 17 UT. The Figure 8 shows just 3 Pc3 pulses indicating the recovery phase of a geomagnetic storm. The Figure 9 and 10 shows, respectively, the spectrograms of the interval 16-17 UT and 7.5-8.5 UT of the day 26. The amplitudes of KOU, ARA and TTB present an amplification compared to the amplitude of SJG. This happens due to EEJ and the recovery phase of the geomagnetic storm.

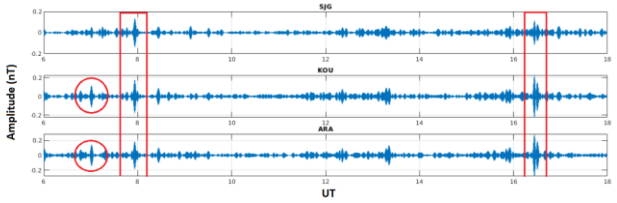

Figure 7 - Identification of Pc3 pulses in the day 26. Red rectangles identify the pulses

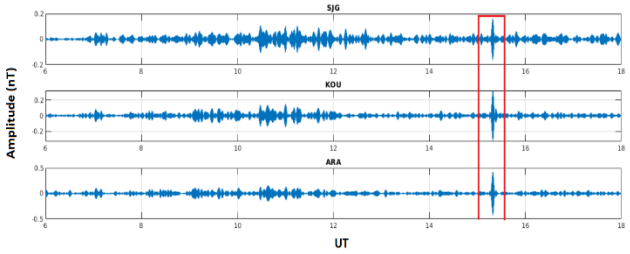

Figure 8 - Identification of Pc3 pulses in the day 27. Red rectangles identify the pulses

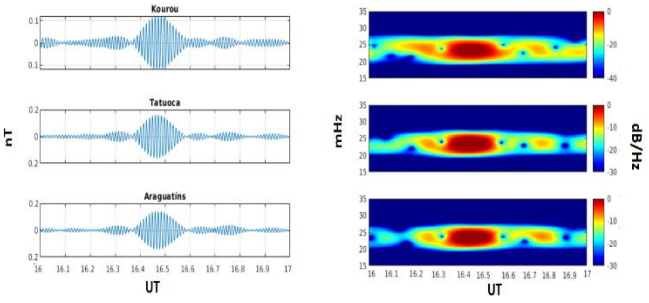

Figure 9 - Pc3 spectrogram of the day 26 between 16 UT and 17 UT.

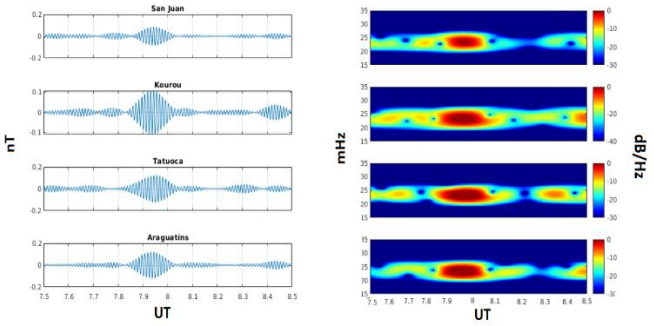

Figure 10 - Pc3 spectrogram of the day 26 between 7.5 UT and 8.5 UT.

The Figures 11, 12 and 13 show the magnetic profiles of days 21, 22 and 23 for Pc4, respectively. The quiet days showed just a Pc4 pulse for the day 21 between 15 UT and 16 UT (red rectangle of Figure 11). The days 22 and 23 show incompatibility of signals when they are compared with different stations. The Figure 14 shows the spectrogram of Figure 11. The dB/Hz ratio creates a 'belt' of values between 7 and 15 mHz, denoting the frequency range of a Pc4 pulse. We realized an increase of TTB values compared to near stations, this is explained by the EEJ influence.

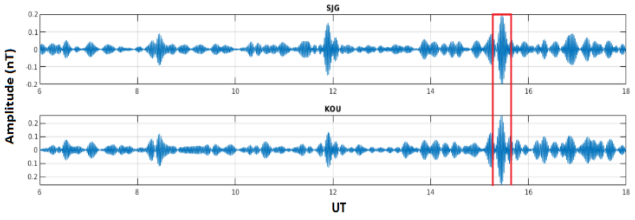

Figure 11 - Identification of Pc4 pulses in the day 21. Red rectangles identify the pulses.

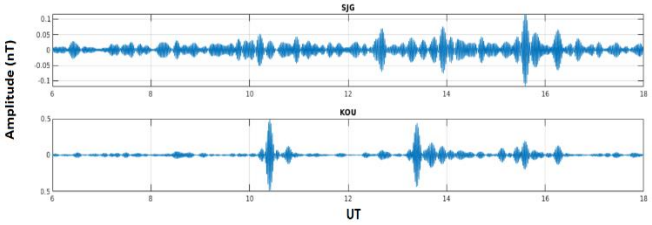

Figure 12 – Magnetic profile of the day 22. No Pc4 pulses were found.

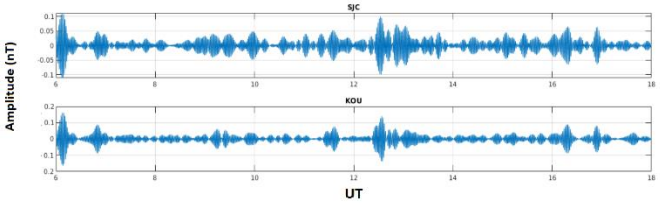

Figure 13 – Magnetic profile of the day 23. No Pc4 pulses were found.

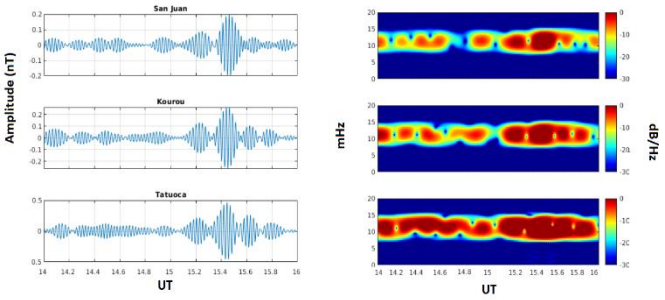

Figure 14 – Pc4 spectrogram of the day 21 between 14 UT and 16 UT.

We detected 6 Pc4 pulses in the disturbed days. The day 25 did not show any Pc4 pulse, just noisy data with amplitudes less than 0.2 nT. The day 26 and 27 showed 3 Pc4 pulses each (Figure 15 and 16, respectively). Day 26 presented pulses between 12 UT and 14 UT and day 27 presented pulses between 10 UT and 12 UT. Day 26 is under main phase of the geomagnetic storm and day 27 is under recovery phase. The Figures 17 and 18 show the spectrogram of Figures 14 and 15, respectively.

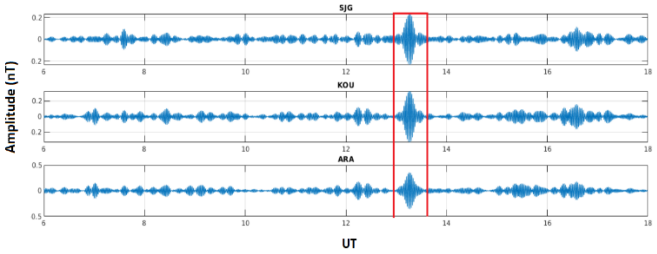

Figure 15 – Identification of Pc4 pulses of the day 26.

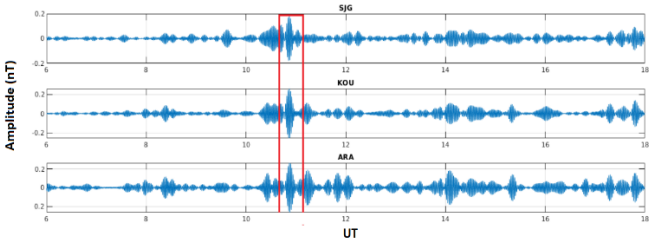

Figure 16 – Identification of Pc4 pulses of the day 27.

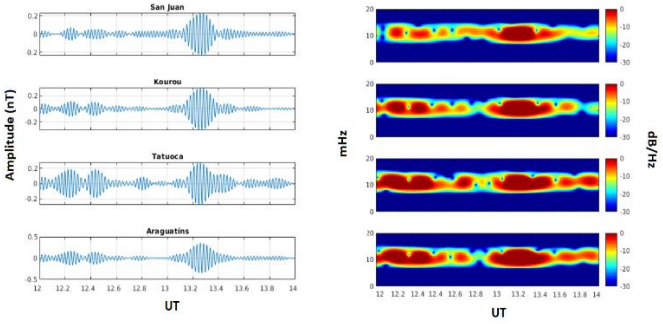

Figure 17 – Pc4 spectrogram of the day 26 between 12 UT and 14 UT.

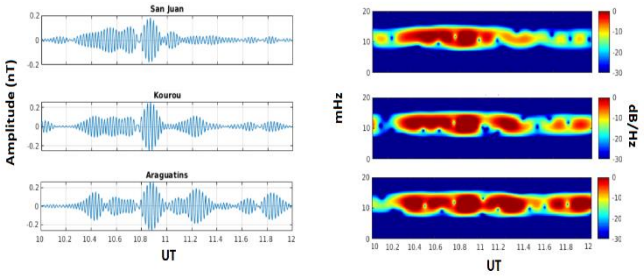

Figure 18 – Pc4 spectrogram of the day 27 between 10 UT and 12 UT.

Discussions

One of the hypotheses to understand the behavior of Pc3 and Pc4 pulses is the Cowling conductivity (HUGHES and SOUTHWOOD,1976). The ionospheric conductivity has three components described as: horizontal component of the magnetic field, σ_0, electric field vector perpendicular to magnetic field, σ_1, electric field vector perpendicular to both, σ_2. These components are expressed as

$$\sigma_0 = Ne^2\left[\frac{1}{m_e v_e} + \frac{1}{m_i v_i}\right], \tag{3}$$

$$\sigma_1 = Ne^2\left[\frac{v_e}{m_e(v_e^2 + \Omega_e^2)} + \frac{v_i}{m_i(v_i^2 + \Omega_i^2)}\right], \tag{4}$$

$$\sigma_2 = Ne^2\left[\frac{\Omega_e}{m_e(v_e^2 + \Omega_e^2)} + \frac{\Omega_i}{m_i(v_i^2 + \Omega_i^2)}\right], \tag{5}$$

where the subscripts ‘e’ and ‘i’ denote respectives electrons and ions, v_e and v_i are collisions frequencies, Ω_e and Ω_i are cyclotronic frequencies, m_e and m_i are masses, e is the elementary charge and N is the electronic density.

The longitudinal conductivity (equation 3) describes the particles of the electronic charges along the extension of the geomagnetic field in the presence of an electric field. When the components of the electric field are perpendicular to a magnetic field, the conductivity parallel to the current flow is defined as Perdersen conductivity (equation 4) and the conductivity orthogonal to the current flow is defined as Hall conductivity (equation 5).T he Cowling conductivity, σ_c, is function of all parameters mentioned and it is defined as

$$\sigma_c = \sigma_1 + \frac{\sigma_2^2}{\sigma_1}. \tag{6}$$

According to Roy and Rao (1998) there is not a unified answer in literature about the origin of the geomagnetic pulsations, however Sarma and Sastry (1995) have stated that pulsations on magnetic equator are related to the presence of a constant ionospheric current flow. Theories about the E region of ionosphere showed that the effects of amplitudes variation of the pulses at the magnetic equator are function of the Cowling conductivity

(KIKUCHI, ARAKI, 1979a,b; ITONAGA et al., 1998). The pulses are related to the upstream waves (generated by ionic cyclotron instabilities on the magnetoshphere bowshock) that propagate along the equatorial region of the magnetosphere. The increase of Cowling conductivity in this latitude is responsible for the damping effect in the pulse signals.

Conclusions

We studied the behavior of Pc3 and Pc4 type pulsations on geomagnetically quiet and disturbed days. In addition, we chose stations closer to the magnetic equator to characterize the effect of EEJ on these pulsations. We use bandpass filtering and the use of spectrograms to identify Pc3 pulsations and Pc4 on 21, 22, 23, 25, 26 and 27 of August, 2018. The results found may contribute to the understanding of the mechanism that changes the amplitudes of the signals detected in the region of the magnetic equator. For future investigations we recommend the use of power density to quantify the amplification and damping of pulse amplitudes. Furthermore, the lack of coverage of stations in the Amazon decreased the details of the variation of pulsations, so we recommend the use of more data of the equatorial region.

Acknowledgments

The authors acknowledge Observatorio Nacional (ON) for sharing the data of Tatuoca station and Amanda Piassi and Dr. Clezio de Nardin for the support. G. A. S. Picanço thanks CAPES/MEC (grant 88887.467444/2019-00).

References

CAMPBELL, W. H. Introduction to geomagnetic fields: 2.Ed. Cambridge: Cambridge University Press, 2003. 337 p. ISBN 0521822068.

DUNGEY, J. W. Interplanetary Magnetic Field and the Auroral Zones. Phys. Rev. Lett., American Physical Society, v. 6, n. 2, p. 47–48, jan. 1961.

GONZALEZ, W. D.; JOSELYN, J. a.; KAMIDE, Y.; KROEHL, H. W.; ROSTOKER, G.; TSURUTANI, B. T.; VASYLIUNAS, V. M. What is a geomagnetic storm? Journal of Geophysical Research, v. 99, n. A4, p. 5771–5792, 1994. ISSN 0148-0227.

HUGHES, W. J.; SOUTHWOOD, D. J. The screening of micropulsation signals by the atmosphere and ionosphere. Journal of Geophysical Research, v. 81, n. 19, p. 3234–3240, 1976

ITONAGA, M.; YOSHIKAWA, A.; YUMOTO, K. Transient response of the nonuniform equatorial ionosphere to compressional MHD waves. J. Atmos. Sol.-Terr. Phys., v. 60, p. 253-261, 1998.

JACOBS; J.A., KATO, Y.; MATSUSHITA, S.; TROITSKAYA, V.A. Classification of geomagnetic micropulsations. Journal of Geophysical Research, v. 69, n. 1, p. 180- 181, 1964. doi:10.1029/JZ069i001p00180

KAMIDE, Y.; CHIAN, A. Handbook of the Solar-Terrestrial Enviroment. Berlim: Springer, 2007.

KELLEY, M. C. The earth's ionosphere: plasma physics and electrodynamics. 2. ed. Burlington: Academic Press, 2009. International Geophysics Series, v. 96.

KIKUCHI, T.; ARAKI, T. Horizontal transmission of the polar electric field to the equator. Journal of Atmospheric and Terrestrial Physics, v. 41, n. 9, p. 927 – 936, 1979b. doi: 10.1016/0021-9169(79)90094-1.

McPHERRON, R. L. Magnetic Pulsations: their sources and relation to solar wind and geomagnetic activity. Surveys in Geophysics, v. 36, n. 5, p. 545-592, 2005. doi: 10.1007/s10712-005-1758-7.

PIASSI, A. R. Análise de pulsações magnéticas Pc3 e Pc4 na região da anomalia magnética do Atlântico Sul. Dissertação (Mestrado em Geofísica Espacial) - Instituto Nacional de Pesquisas Espaciais, São José dos Campus, 2018.

ROY, M.; RAO, D. R. K. Frequency dependence of equatorial electroject effect on geomagnetic micropulsations. Earth Planets Space, v. 50, n. 10, p. 847 – 851, 1998. doi: 10.1186/BF03352178.

SAITO, T. Geomagnetic pulsations. Space Science Reviews, v. 10, n. 3, p. 319–412, 1969. ISSN 00386308.

SAMSON, J. C. Geomagnetic pulsations and plasma waves in the Earth's magnetosphere. In: JACOBS, J. A. (ed.). Geomagnetism. London: Academic Press, p. 481-591, 1991.

SARMA, S.V.S.; SASTRY, T.S. On the equatorial electrojet influence on geomagnetic pulsation amplitudes. Journal of Atmospheric and Terrestrial Physics, v. 57, n. 7, p. 749-754, DOI: 10.1016/0021-9169(94)00053-Q,

SHINOHARA, M.; YUMOTO, K.; YOSHIKAWA, A.; SAKA, O.; SOLOVYEV, S. I.; VERSHININ, E. F.; TRIVEDI, N. B.; DA COSTA, J. M.; The 210◦ MM Magnetic Observation Group. Wave characteristics of day time and night time Pi2 pulsations at the equatorial and low latitudes. Geophys. Res. Lett., v. 24, n.18, p. 2279 – 2282, 1997. doi: 10.1029/97GL02146.

SIBECK, D. G. Transient quasi-periodic (5 - 15 min) events in the outer magnetosphere. In: ENGEBRETSON, M. J.; TAKAHASHI, K.; SCHOLER, M. (eds.) Solar wind source of magnetospheric ultra-low-frequency waves. AGU Geophysical Monography, v.81, p.173 – 182, 1994. doi: 10.1029/GM081p0173.

SILVA, G.B.D. Caracterização da amplitude de pulsações magnéticas observadas em região sob influência do eletrojato equatorial. Dissertação (Mestrado em Geofísica espacial)- Instituto Nacional de Pesquisas Espaciais, São José dos Campus, 2017.

SIMOES, M. C. Identificação de distúrbios em magnetogramas associados a tempestades magnéticas utilizando ténicas wavelets. 2011. 147 p. Tese (Dissertação de Mestrado) — Instituto Nacional de Pesquisas Espaciais - INPE, São José dos Campos, 2011.

TAVARES, M.; SANTIAGO, M.A.M. Eletricidade atmosférica e fenômenos correlatos. 2002. Revista Brasileira de Ensino de Física. vol.24.n4.